Journal of Magnetic Resonance **140,** 477–481 (1999)
Article ID jmre.1999.1873, available online at http://www.idealibrary.com on IDEAL®

COMMUNICATIONS

Magnetic Resonance Imaging Measurement of Volume Magnetic Susceptibility Using a Boundary Condition

Zhiyue J. Wang,*[,1] Shuchun Li,† and John C. Haselgrove*

**Department of Radiology, The Children's Hospital of Philadelphia, Philadelphia, Pennsylvania 19104; and †Department of Radiology, The University of Pennsylvania Medical Center, Philadelphia, Pennsylvania 19104*

Received December 30, 1998; revised June 23, 1999

A magnetic resonance imaging method is described for measuring the magnetic susceptibility difference between two homogeneous macroscopic compartments in contact with each other. A boundary condition is derived for the interface of the two compartments. This boundary condition predicts that across the interface there is a resonant frequency jump, which is a function of interfacial orientation relative to B_0 field and the difference in susceptibility of the two sides. Based on this relationship, the magnetic susceptibility difference between two materials can be obtained from MR gradient echo imaging using signals from both sides in the vicinity of the boundary. This method is demonstrated by solution phantom experiments.

Key Words: **magnetic resonance imaging; magnetic susceptibility; boundary condition.**

Measurements of tissue magnetic susceptibility have important medical applications. Brittenham *et al.* showed that liver susceptibility measurement by a superconducting quantum interference device (SQUID) can be used to evaluate iron overload (*1*). Iron overload occurs in a variety of diseases (*2, 3*) and may lead to organ failure and death. In humans, there is no pathway to excrete excess amount of iron in the body and this iron is stored in the liver, heart, bone, and various other organs. Although numerous papers have been published correlating the tissue iron level with nuclear spin relaxation rates 1/T1 and 1/T2, iron levels obtained from susceptibility measured by the SQUID have been considered by many experts to be more reliable. The ability to quantify tissue magnetic susceptibility *in vivo* by MRI will lead to the development of new techniques for the measurement of tissue iron concentration. MRI can be readily applied to the heart and other organs where information of tissue iron levels is important but so far has been elusive to clinicians.

For decades, NMR spectrometers have been used to measure the susceptibility of solutions. In these measurements, the solution is contained in a specially constructed tube so that the magnetic field within the sample is uniform, and the relationship between the NMR frequency shift and susceptibility is known. MR imaging is able to map out spatial distribution of the magnetic field and can be used to measure the magnetic susceptibility of materials in a more flexible manner (*4, 5*). However, most published work either requires that the sample has a regular shape for which the pattern of field distribution is known or invokes complicated mathematical analysis to compute the field distribution for a system with an irregular shape. In the *in vivo* measurement of human organs such as liver, it is possible to calculate the magnetic field distribution induced by the organ provided that its geometry is determined (*6*). However, the computation involved is tedious, and the results of human studies have not been reliable. This paper describes an MRI susceptibility measurement method which takes advantage of a resonant frequency discontinuity at the interface between two materials, each having observable MR signal. The susceptibility difference between the two materials can be obtained using data obtained from the vicinity of the interface without knowing all details of the sample geometry.

Since the resonant frequency depends both on the volume magnetic susceptibility and on the static field in the magnet, the frequency shift due to susceptibility can be measured by comparing the frequency of the material under investigation with that of a reference material. The approach described here focuses our attention on the interfacial regions only. The boundary conditions of the Maxwell Equations determine the difference of magnetic field across the interface. Therefore, the susceptibility difference between two materials can be obtained from the difference in resonant frequency across the interface without the knowledge of the field distribution in other regions. The only geometric information needed is the angle between the interface and the external magnetic field.

Consider two homogeneous compartments in contact with each other labeled as "1" and "2" (Fig. 1), each containing a solution or soft tissue. The static magnetic field $\mathbf{B}_0$ is along the

[1] To whom correspondence should be addressed. E-mail: wang@email.chop.edu.

1090-7807/99 $30.00

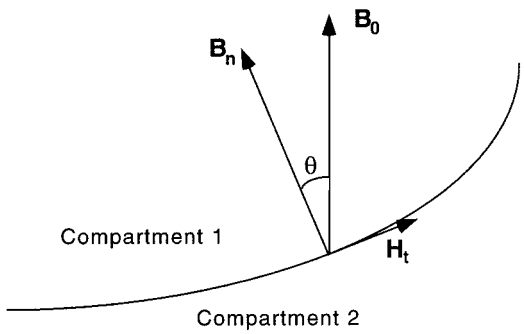

FIG. 1. A sketch of compartment interface. The curved line represents the boundary between compartment 1 and compartment 2. The static magnetic intensity $\mathbf{B}_0$ is along the z direction, and the B field along the interface normal direction is denoted $\mathbf{B}_n$. The angle between $\mathbf{n}$ and $\mathbf{B}_0$ is θ. The interface tangential direction in the plane determined by $\mathbf{B}_0$ and $\mathbf{n}$ is denoted $\mathbf{t}$, and the magnetic field along the tangential direction is $\mathbf{H}_t$. The vectors $\mathbf{n}$ and $\mathbf{t}$ are not shown in the figure.

z direction, and the interface normal direction is denoted $\mathbf{n}$. The angle between $\mathbf{n}$ and $\mathbf{B}_0$ is θ. The interface tangential direction in the plane determined by $\mathbf{B}_0$ and $\mathbf{n}$ is denoted $\mathbf{t}$. According to the boundary conditions of the Maxwell Equations, the $\mathbf{B}$ field along $\mathbf{n}$, and the $\mathbf{H}$ field along $\mathbf{t}$, across the interface is continuous. That is,

$$B_{n1} = B_{n2} = B_n \quad [1]$$

$$H_{t1} = H_{t2} = H_t. \quad [2]$$

The B and H in Eqs. [1] and [2] are the macroscopic fields, and

$$\mathbf{B} = \mathbf{H} + 4\pi\mathbf{M} \quad [3]$$

$$\mathbf{M} = \chi\mathbf{H}. \quad [4]$$

Here $\mathbf{M}$ is the magnetization and χ is the volume magnetic susceptibility (*7*). Since χ is very small ($\chi \ll 1$), we are justified to ignore χ^2 terms and derive a linear relationship. Therefore, we can assume $\mathbf{M}_i$ ($i = 1$ or 2, for the two compartments) to be in the z direction. The z component of the $\mathbf{B}$ field can be expressed in terms of B_n and B_t (the tangential component of the B field) for compartments 1 and 2 at the interface,

$$B_{zi} = B_n\cos\theta + B_{ti}\sin\theta \quad (i = 1, 2). \quad [5]$$

In Eq. [5], B_{ti} can be expressed in terms of H_t and $\mathbf{M}_i$ projected along the tangential direction:

$$B_{ti} = H_t + 4\pi M_i\sin\theta \quad (i = 1, 2). \quad [6]$$

Substitute Eq. [6] into Eq. [5] and obtain

$$B_{zi} = B_n\cos\theta + (H_t + 4\pi M_i\sin\theta)\sin\theta \quad (i = 1, 2). \quad [7]$$

From Eq. [7], it is easy to show that the difference in the z component of the $\mathbf{B}$ field in the two sides of the boundary is

$$\Delta B_z = 4\pi\sin^2\theta\Delta M. \quad [8]$$

Here $\Delta B_z = B_{z2} - B_{z1}$, $\Delta M = M_2 - M_1$. The resonant frequency of the nucleus spin, ν, is determined by the local field B_{local} experienced by the spin,

$$\nu = \gamma B_{\text{local}}/2\pi. \quad [9]$$

$\mathbf{B}_{\text{local}}$ is different from the macroscopic fields in Eqs. [1]–[8]. The relationship of the macroscopic field and local field can be found in standard textbooks (*7*). The same relationship holds for solids with well-defined crystal structures and liquids or soft tissues where the motion of molecules is completely random. The local field is obtained by correcting the macroscopic field with a Lorentz term $-(8\pi/3)\mathbf{M}$ (*4*):

$$\mathbf{B}_{\text{local}} = \mathbf{B} - \frac{8\pi}{3}\mathbf{M}. \quad [10]$$

Although the difference between the local field and the macroscopic field may seem difficult to explain at first glance, Eq. [10] can be understood in very simple terms. The local field $\mathbf{B}_{\text{local}}$ can be divided into two parts, a near field contribution and a far field contribution. The near field arises from molecules within a sphere centered at the nuclear spin (the so-called sphere of Lorentz) and sources outside the sphere contribute to the far field. The far field contribution is a macroscopic field accurately described by the equations of macroscopic fields. It is the near field contribution which needs to be reevaluated. According to the macroscopic field model, a uniformly magnetized sphere contributes to its center a field of $(8\pi/3)\mathbf{M}$. However, the true near field contribution from molecules inside the Lorentz sphere to the center of the sphere is zero. Therefore, a term $-(8\pi/3)\mathbf{M}$ needs to be added to the macroscopic field to obtain the local field.

From Eqs. [8]–[10], and considering $\mathbf{M} \approx \chi\mathbf{B}$ (because $\chi \ll 1$), it is straightforward to derive the relationship between the difference of susceptibility $\Delta\chi = \chi_2 - \chi_1$ and the difference in frequency shift $\Delta\nu = \nu_2 - \nu_1$ across the boundary:

$$\frac{\Delta\nu}{\nu_0} = \frac{4\pi}{3}\Delta\chi(1 - 3\cos^2\theta). \quad [11]$$

Here ν_0 is the radiofrequency carrier frequency. Equation [11] implies that the change in frequency across the interface occurs as a sudden jump. In this derivation we did not include effects of the hyperfine shift (*8*) which comes from the Fermi contact interaction between unpaired electron spin and nucleus (*9*) in solvent. To include the effects of the hyperfine shift, Eq. [11] can be modified by adding to the right-hand side a θ indepen-

dent term which is proportional to magnetic solute concentration:

$$\frac{\Delta\nu}{\nu_0} = \frac{4\pi}{3}\Delta\chi\{(1 - 3\cos^2\theta) + S_{hs}\}. \quad [12]$$

S_{hs} can be determined experimentally by studying the θ dependence of $\Delta\nu/\nu_0$.

The size of the frequency jump across the interface is determined only by the properties of magnetic media at the surface. Field sources not in the vicinity of the surface point contribute to the field on both sides of the surface, but the contribution is continuous across the surface. This is why the boundary condition Eq. [12] depends only on the orientation of the surface and the difference of susceptibility of the two sides. For a homogeneous ellipsoid of revolution placed in uniform external magnetic field, analytical solutions of the magnetic field exist (*8*). A point on a smooth surface can always be characterized by two principal curvature radii along two orthogonal directions. Therefore, the behavior of the field near surface is similar to that near a ellipsoid of revolution. The curvature of the surface determines the gradient of the induced field and larger curvatures (smaller curvature radii) will induce a stronger field gradient. However, Eq. [12] remains valid when the surface is curved. A good example is a sphere which is the simplest special case of an ellipsoid, and the validity of Eq. [12] can be directly verified. For a uniformly magnetized sphere in a homogenous external field, the induced field is uniform inside the sphere but behaves as a dipole field outside the sphere, with a radial spatial dependence of $1/r^3$ away from the center.

A MRI measurement of magnetic susceptibility can be made based on Eq. [12]. Several conditions need to be fulfilled for this relationship to be valid in an imaging study. First of all, the ruggedness of the surface needs to be negligible. We may require the length scale of local ruggedness to be smaller than the image pixel size. This condition is satisfied for our intended *in vivo* applications because organs usually have smooth surfaces. Second, assuming the surface is smooth, the relationship Eq. [12] is exact only for locations infinitely close to the interface due to the nature of a boundary condition. When the curvature radii of the interface are much larger than the image pixel and assuming shimming is favorable, the magnetic field near the interface does not change significantly near the interface and Eq. [12] is a good approximation for pixels near the boundary. When significant curvatures exist for the surface, the field near the interface is expected to change significantly. The field value at the interface may be extrapolated from pixels near the surface, and Eq. [12] may be used with the extrapolated boundary values to measure the susceptibility difference of the two compartments. This method may be suited for susceptibility measurement of various organs and tissues *in vivo*. For example, susceptibility of the heart may be measured using intercostal muscle as reference, which has a constant iron level. An external reference, such as a bag of water, may be used to study surface regions of the human body. Of course, accurate measurement of the susceptibility difference by MRI will become increasingly difficult when the surface curvatures become larger.

TABLE 1

Effects of Shell with Finite Thickness on the Measured Susceptibility for an Infinitely Long Cylindrical Shell Perpendicular to External Magnetic Field

Shell thickness	χ_2 (susceptibility of the shell)	Calculated χ_1	Calculated S_{hs}
0.0 mm	—	1.00×10^{-6}	0.00
	1.0×10^{-6}	1.00×10^{-6}	0.00
1.0 mm	0.0×10^{-6}	0.95×10^{-6}	−0.03
	-1.0×10^{-6}	0.90×10^{-6}	−0.05

Note. See text for detail and other parameters.

In practical measurement, it is often unavoidable that there is a thin layer of a third tissue or material in between the two compartments of interest. This layer will have some effect on the outcome of the measurement. However, if the layer is thin and the magnetic field does not vary significantly across the layer, the continuity conditions of B_n and H_t in the two compartments of interest remain valid despite the presence of a thin layer, and Eq. [12] may still be a good approximation. We have carried out a calculation for an infinitely long cylindrical shell with the long axis perpendicular to the uniform external magnetic field to mimic the situation of the $CuSO_4$ solution experiment described later. We used outer radius $r_2 = 4.0$ cm and inner radius $r_1 = 3.9$ or 4.0 cm, which correspond to shell thickness 1 and 0 mm, respectively. We assumed that the space outside of the cylinder was filled with a reference solution with $\chi_3 = 0.00 \times 10^{-6}$. Inside the cylinder we have a solution $\chi_1 = 1.00 \times 10^{-6}$, and there is no hyperfine shift on either side. The MR frequency differences between $r = r_2$ and $r = r_1$ at different θ values were calculated analytically. We thus obtained a simulated θ dependence of $\Delta\nu/\nu_0$. A least-squares curve fit of Eq. [12] on the simulated data allowed us to calculate the measured χ_1 and S_{hs} for different shell susceptibility χ_2. The result of the calculation is listed in Table 1. When the wall thickness was zero, error free results were obtained. The presence of a wall with finite thickness introduced error in both χ_1 and S_{hs}. The error also depended on the susceptibility of the wall. In Table 1, the largest error is associated with the shell susceptibility most different from those of the two compartments. Based on these calculations, we may expect that systematic errors may be tolerable for *in vivo* cardiac iron measurements using intercostal muscle as a reference.

Many techniques have been described for measuring magnetic field. The use of phase to measure change in susceptibil-

ity has been reported previously (*10*). In particular, the phase contrast method or modified Dixon method has been often used to measure changes in B_0 or resonant frequency based on the change of phase of the signal (*11*, *12*). Normally the phase change is converted to intensity contrast but would give an equally accurate answer as phase signal. In addition, the same experiment could be performed using image tagging methods (*13*). However, for our intended application, the use of phase image acquired with a gradient echo pulse sequence for quantitation is appropriate. The implementation of the pulse sequence is very simple. Compared with the Dixon method, one set of gradient echo images is sufficient because we are only concerned about the phase difference. Furthermore, the results are independent of T1 and T2 relaxation times, which are known to change drastically for tissue overloaded with iron.

Solution phantom experiments were carried out to verify the theory. All MR studies were performed on a Siemens Magnetom Vision 1.5 T whole body clinical MRI scanner ($\nu_0 = 63.6$ MHz) using a circularly polarized extremity coil. All samples were at room temperature (21°C). Experiments were performed using gradient echo imaging techniques, which do not refocus phase changes caused by field inhomogeneity. Both amplitude and phase images were recorded.

The first experiment verified both the size and angular dependence of $\Delta\nu/\nu_0$ across the interface predicted by Eq. [12]. The experimental setup used a phantom with two compartments, containing water and copper sulfate solution, respectively. Solution of $CuSO_4$ (0.3 M) in a thin cylindrical plastic bottle (wall thickness = 1 mm, outer diameter = 80 mm) was immersed in a water bath, with the bottle axis along the vertical direction (y axis). Multi-slice gradient echo images (TR = 10 ms, TE = 4.2 ms with asymmetric echo, flip angle = 8°, field of view = 200 mm, slice thickness = 5 mm, matrix size 256 × 256, 12 slices with number of average = 25) were acquired in the xz plane.

The image data were transferred to a SUN SPARC workstation and processed by home written software using IDL (Research System Inc., Boulder, CO). Because of the use of asymmetric echo, the phase images have a linear phase ramp. This phase ramp was first removed as follows. The complex data were reverse Fourier transformed back into the k-space. The k-space data were shifted so that the peak signal was in the center. The k-space data were then transformed back into the image space. The phase maps were obtained from the imaginary part of the logarithm of the complex images. The phase ranged from $-\pi$ to π in the phase maps. However, the phase changes due to the susceptibility effects were larger than this range, and consequently phase wrap-around remained a problem. Software was again used to make necessary adjustments to correct the phase wrap. The algorithm is as follows: the software compares the phase image data matrix along each direction, pixel by pixel. When it finds that the phase difference between the two adjacent pixels is greater than a threshold value (we can "arbitrarily" assign this threshold value) such as 1.5π, it added 2π to all other pixels beyond this pixel. Similarly, the software subtracts 2π from all other pixels beyond this pixel, if they differ by -1.5π.

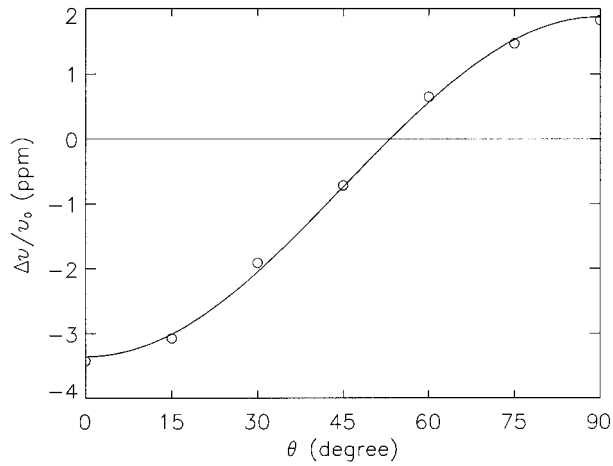

FIG. 2. Experimental verification of Eq. [12] using a phantom with two compartments, containing water and copper sulfate solution, respectively. The circles represent experimental data and the solid line is obtained from the least-squares curve-fit using Eq. [12]. The least-squares estimation resulted in a mass magnetic susceptibility of $\chi_M = 1.39 \times 10^{-3}$ cm^3/mol for solute $CuSO_4$ and a hyperfine shift of $S_{hs} = 0.074$.

Water proton signal phase jump across the interface was measured for θ from 0° to 90° in 15° increments. The software rotated the images by θ input by the operator, so that the resultant image has a horizontal interface for the point of interest. The software allowed the operator to define the position of tissue interface by a mouse, based on the image displayed on the computer screen. Then the computer mouse was used to select the regions on both sides of the interface where data were used for analysis. Typically, one region was a rectangular box (2 pixels × 8 pixels) with long axis along the tangential direction of interface. A second-order polynomial was used to fit the data points in both regions and extrapolated a phase jump value $\Delta\phi$ across the interface. The difference in resonant frequency $\Delta\nu$ was calculated from $\Delta\phi/(2\pi \cdot TE)$. For each angle θ, $\Delta\nu$ was averaged over values obtained in 12 slices. The frequency difference $\Delta\nu$ across the interface between water and the copper sulfate solution was then evaluated at different θ values. Figure 2 shows $\Delta\nu/\nu_0$ versus θ. The circles represent experimental data and the solid line is obtained from the least-squares estimation using Eq. [12]. The least-squares estimation resulted in a mass magnetic susceptibility of $\chi_M = 1.39 \times 10^{-3}$ cm^3/mol for solute $CuSO_4$ and a hyperfine shift of $S_{hs} = 0.074$. The resulting susceptibility agreed well with a mass magnetic susceptibility of $\chi_M = 1.33 \times 10^{-3}$ cm^3/mol for $CuSO_4$ (*14*).

Our intended practical application is to measure tissue iron levels. Most of the tissue iron is stored in the form of ferritin and hemosiderin. Therefore, in the second experiment we tested the theory on a ferritin solution.

A phantom was constructed which contained, in two com-

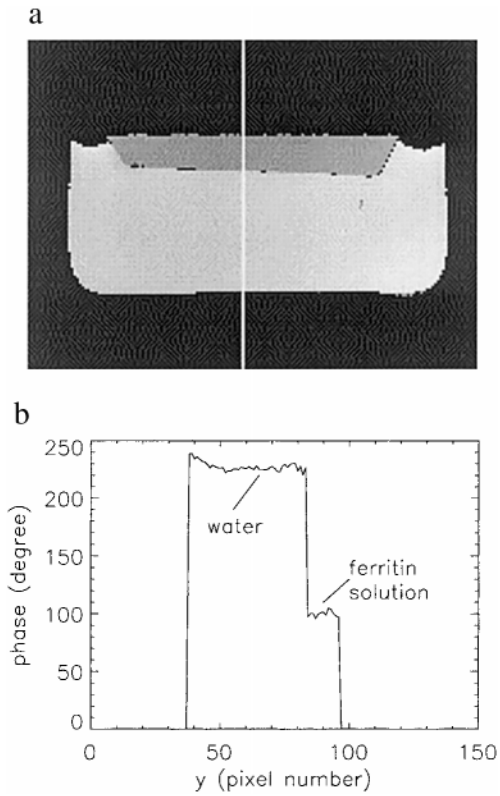

FIG. 3. Experimental verification of Eq. [12] using a phantom with two compartments, containing water and ferritin solution, respectively. (a) shows a portion of the phase image. The water in the figure spans 6.7 cm from left to right. The phase for regions outside the phantom is set to zero. A second-order polynomial has been added to the phase image to remove the variations due to factors not related to the interface. The bright vertical line in (a) indicates the location of the phase profile in (b). There is a 130° phase jump at the interface between water and ferritin solution in (b), corresponding to $\chi_M = 1.13 \times 10^{-4}$ cm^3/g Fe for ferritin iron.

partments, water and ferritin solution, respectively. Horse spleen ferritin solution (Sigma, 1400 iron atom per ferritin molecule) was diluted to 1.2 mg Fe/mL. The solution was contained in a weighing boat which was positioned above water. Thus a flat interface was created in the *xz* plane ($\theta = 90°$). Transverse gradient echo phase and amplitude images ($TR = 40$ ms, $TE = 10$ ms, flip angle = 15°, fov = 128 mm, slice thickness = 3 mm, matrix size 256×256) was acquired in the *xy* plane (Fig. 3). The discontinuity of the resonant frequency at the interface is apparent in Fig. 3. The phase jump between the two compartments was $\Delta\phi = 130°$ (Fig. 3b) for $\theta = 90°$. Ignoring the hyperfine shift, we deduced $\chi_M = 1.13 \times 10^{-4}$ cm^3/g Fe, which agreed well with a literature value of 1.16×10^{-4} cm^3/g Fe for ferritin (*15*).

We introduce a magnetic resonance imaging method to measure the difference of volume magnetic susceptibility of two materials in contact with each other. One material with known susceptibility may be considered as a reference in order to obtain the susceptibility of the second material. This method is new compared with previous techniques in that data analysis utilizes a boundary condition derived from the boundary conditions of the Maxwell Equations. Contributions from materials away from the interface do not need to be considered explicitly. The experimental results presented here demonstrate that the method is valid for solutions. Future work will test the validity of this method on biological tissues overloaded with iron.

ACKNOWLEDGMENTS

ZJW and JCH receive support from NIH Grant R01 HL61182-01. SL is supported by NIH research resource center Grant RR-02305 and by Department of Defense training Grant DAMD 17-94-J-4027. We thank Dr. Alan Cohen for initiating our research on tissue iron overload.

REFERENCES

1. G. M. Brittenham, D. E. Farrell, J. W. Harris, E. S. Feldman, E. H. Danish, W. A. Muir, J. H. Tripp, and E. M. Bellon, Magnetic-susceptibility measurement of human iron stores, *N. Engl. J. Med.* **307,** 1671–1675 (1982).
2. L. M. Buja and W. C. Roberts, Iron in the heart: etiology and clinical significance, *Am. J. Med.* **51,** 209–221 (1971).
3. G. W. Richter, The iron loaded cell—cytopathology of iron storage, *Am. J. Pathol.* **91,** 362–404 (1978).
4. S. C. K. Chu, Y. Xu, J. A. Balschi, and C. S. Springer, Bulk magnetic susceptibility shifts in NMR studies of compartmentalized samples: use of paramagnetic reagents, *Magn. Reson. Med.* **13,** 239–262 (1990).
5. O. Beuf, A. Briguet, M. Lissac, and R. Davis, Magnetic resonance imaging for the determination of magnetic susceptibility of materials, *J. Magn. Reson. Series B* **112,** 111–118 (1996).
6. R. W. Holt, P. J. Diaz, J. L. Duerk, and E. M. Bellon, MR susceptometry: An external phantom method for measuring bulk susceptibility from field-echo phase reconstruction maps, *JMRI* **4,** 809–818 (1994).
7. J. D. Jackson, "Classical Electrodynamics," 2nd ed., Wiley, New York (1975).
8. C. S. Springer, Physicochemical principles influencing magneto-pharmaceuticals, *in* "NMR in Physiology and Biomedicine" (R. J. Gillies, Ed.), pp. 75–99, Academic Press, San Diego (1994).
9. C. P. Slichter, "Principles of Magnetic Resonance," 3rd ed., Springer-Verlag, New York (1990).
10. R. M. Weisskoff and S. Kiihne, MRI susceptometry: image-based measurement of absolute susceptibility of MR contrast agents and human blood, *Magn. Reson. Med.* **24,** 375–383 (1992).
11. H. N. Yeung and D. W. Kormo, Separation of true fat and water images by correcting magnetic field inhomogeneity in situ, *Radiology* **159,** 783–786 (1986).
12. G. H. Glover and E. Schneider, Three point Dixon method for true water/fat decomposition with B_0 inhomogeneity correction, *Magn. Reson. Med.* **18,** 371–383 (1991).
13. T. J. Mosher and M. B. Smith, Magnetic susceptibility measurements using a double-Dante tagging (DDT) sequence, *Magn. Reson. Med.* **18,** 251–255 (1991).
14. R. C. Weast and M. J. Astle, "CRC Handbook of Chemistry and Physics," 63rd ed., CRC Press, Boca Raton, FL (1982).
15. J. H Bauman and J. W. Harris, Estimation of hepatic iron stores by in vivo measurement of magnetic susceptibility, *J. Lab. Clin. Med.* **70,** 246–257 (1967).